Application of EPMA Analyses in the Haftcheshmeh Cu-Mo Porphyry System as a Chemical Indicator of the Source Magma

Shohreh Hassanpour [1*], Maryam Ahankoub [2]

[1] Department of Geology, Payame Noor University, Tehran, Iran

Https://orcid.org/0000-0002-4779-267X

[2] Department of Geology, Payame Noor University, Tehran, Iran

[*]Corresponding author Email: hassanpour@pnu.ac.ir

Received: 13 February 2023

Revised: 30 August 2023

Accepted: 10 September 2023

DOI: 10.22067/econg.2023.81046.1068

Keywords: Apatite, EPMA, Haftcheshmeh, Cu-Mo Porphyry System, Iran

Abstract

The Haftcheshmeh Cu-Mo porphyry system is located in the Arasbaran magmatic zone in Alborz-Azarbaijan structure zone, northwestern Iran. As ore mineralization occurred mainly in gabbrodiorite and granodiorite porphyry stocks, chemical compositions of rock forming minerals in gabbrodiorite and granodiorite porphyries are used to identify critical vectors of magmatic processes and hydrothermal mineralization related to the formation. All analyzed (magmatic and hydrothermal) apatites saturation temperatures show ranges of calculated temperatures of 830°C to 877°C and pressures of 0.11 to 0.96 Kbar, corresponding to depths of 4

to 10 km and H_2O_{melt} content (3< wt.%), and suggesting a hydrous calc-alkaline magma generated from a deep magmatic source. Analyzed apatite support the ore forming magmas which are oxidized by I type magma with relatively high fO_2. The trend of volatile element variations indicated that primary fluid exsolution probably occurred at temperatures from ~712°C to 842°C and was affected by hydrous and oxidized mafic magma from a deeper part of the magma reservoir. It may result in an extensive magma mixture with fractional crystallization of apatite in the evolved gabbrodiorite and granodiorite magma chambers.

Introduction

Cu-Mo porphyry systems are magmatic and hydrothermal systems that form mainly in active continental margin and, Cu-Au type in island arc settings (Sun et al., 2015). Studying chemical compositions of igneous rock-forming minerals, which are in equilibrium with magma, is an efficient and useful strategy for better understanding the condition of ore-forming systems (Pan et al., 2019). Mineral chemistry can be useful as a petrogenetic indicator in estimating the pressure (P), temperature (T), oxygen fugacity (fO_2), and H_2O content, determining the composition of the melt in the magma chamber, and tracking the evolution of magmatic fluids in associated with ore deposits (Ridolfi & Renzulli, 2012). Apatite $Ca_5(PO_4)_3$(F, Cl, OH) is a porphyry indicator mineral (Piccoli & Candela, 2002). Apatite can be used to quantify the parental magma oxidation state, determinate the magma chemistry, distinguish the barren and fertile magma, and estimate the oxygen fugacity (Azadbakht et al., 2018; Zhong et al., 2021). Moreover, apatite is an essential host for various volatile components, including H_2O, Cl, F, and S (Webster et al., 2004; Zhong et al., 2018).

The Haftcheshmeh porphyry Cu-Mo deposit has located 15 km north of Varzeghan city in the eastern Azarbaijan Province, northwest of Iran, adjacent to Sungun giant Cu-Mo porphyry deposit in Arasbaran magmatic zone, northwest of Iran (Alborz-Azarbaijan structure zone) (Figure 1A&B). The studied area is approximately 10 km2. Given the data from drill holes, the deposit contains 180 Mt of ore reserves with an average Cu grade of 0.46 wt.% and Mo grade of 350 ppm (Hassanpour & Moazzen, 2018; Zaheri-Abdehvand et al., 2022). To better understand the physicochemical conditions of magma evolution and mineralization processes, the chemical compositions of apatite in the gabbrodiorite and granodiorite porphyry stocks of Haftcheshmeh deposit were studied.

Major elements composition and volatile components were investigated by using apatite mineral chemistry within the (Cu-Mo) mineralized intrusions to identify critical vectors of magmatic and hydrothermal processes.

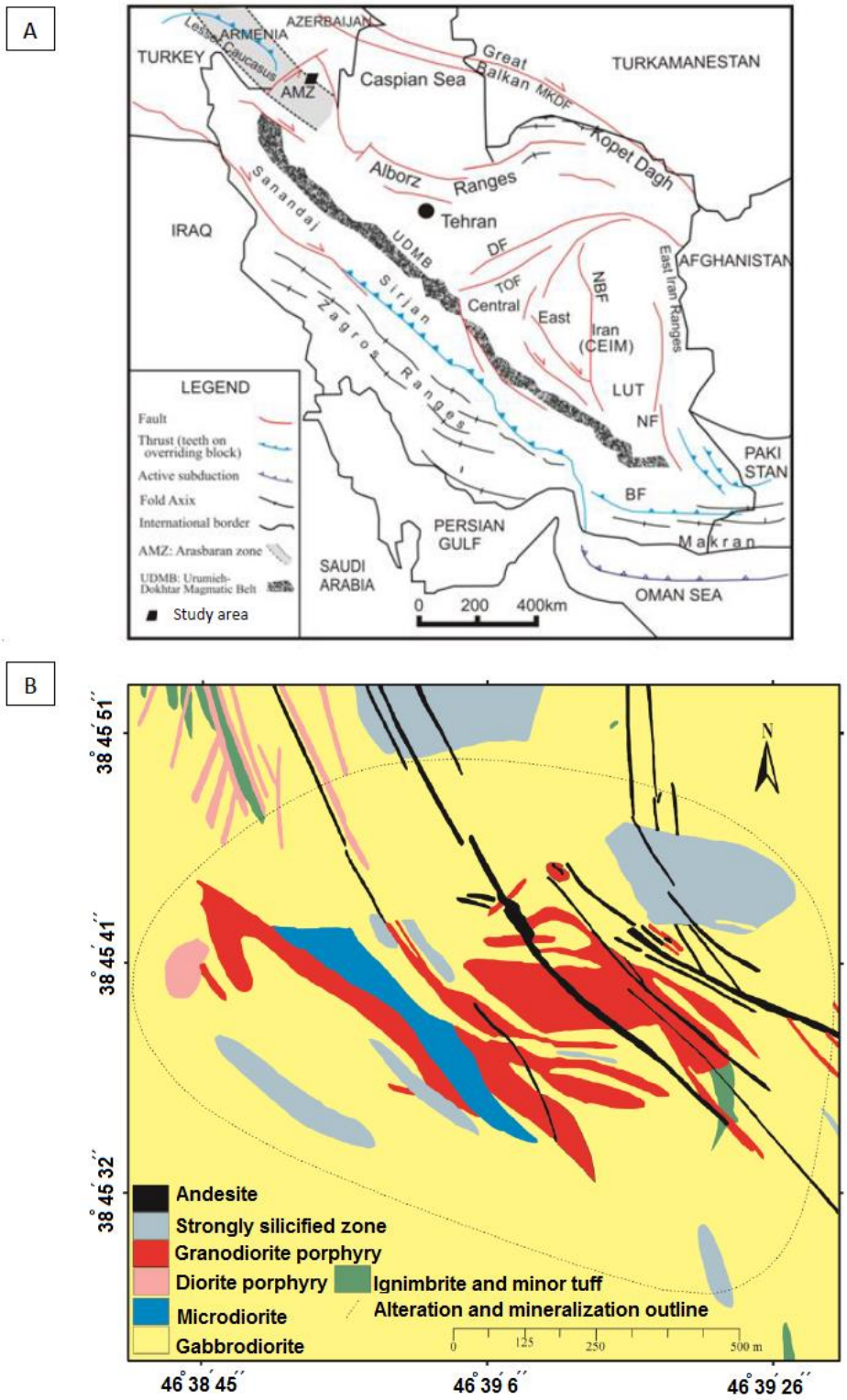

Fig. 1. A: Simplified geology map of Iran (modified from Nabavi, 1976), showing the Haftcheshmeh Cu-Mo porphyry in the Alborz-Azarbaijan structure zone, NW Iran; B: Geological map of the Haftcheshmeh ore deposit (Hassanpour & Moazzen, 2018).

Geological setting

Regional geology

Arasbaran Magmatic Zone is located in the southern margin of the Lesser Caucasus. The geology of the studied area is dominated by the upper Eocene to the upper Pliocene calc-alkaline volcanic and volcano-sedimentary successions overlying the Cretaceous basements consisting of predominantly limestone and pyroclastic rocks. During the Oligocene to the upper Miocene, various granitoid intrusions with calc-alkaline affinities were placed in this region (Hassanpour & Moazzen, 2018; Adeli, 2012; Zaheri-Abdehvand et al., 2022). Haftcheshmeh intrusion with a calc-alkaline affinity formed in an active continental margin (Hassanpour & Moazzen, 2018; Figure 3A&B). Tectono-magmatic events in Arasbaran magmatic zone were responsible for a wide range of ore-forming processes that began in the late Cretaceous at ~110 Ma and terminated at ~4 Ma (UN, 2000; Hassanpour, 2010), and led to the development of a broad magmatic zone, ~100 km width and ~280 km length. Arasbaran volcanic rocks ranged from Eocene to Paleocene in age. Along Arasbaran Magmatic Zone, intrusive rocks intruded into Cretaceous limestone, volcanoclastics and Cenozoic (Paleocene to Miocene) marine sedimentary and minor andesitic volcanic rocks (Mehrparto, 1973; Hassanpour, 2010).

Haftcheshmeh intrusions, together with the lithologically correlative Ordubad and Shayvar Dagh batholiths interpreted as remnants of a magmatic arc constructed along an Andean-type continental margin (Hassanpour, 2010; Hassanpour & Moazzen, 2018).

2. 2. Geology of the Haftcheshmeh deposit

Haftcheshmeh porphyry system is formed in the northwest of Sungun giant Cu-Mo porphyry mine.

Country rocks: The most widespread rock units are the Cretaceous flysch type sediments series, which outcropped in the southern, northwestern, and northeastern parts of the area. These series are covered by Eocene volcanic complexes with andesitic to trachyandesite tuffs in compositions. Intrusive rocks are partly covered by a roof pendant of lithic tuffs, volcanoclastics, and interbedded shale of Upper Cretaceous age, partly converted to hornfels, especially in beside of stocks (Figure 2A; Hassanpour, 2010).

Intrusive rocks: Magmatism was the most intensive in the late Oligocene and early Miocene, resulting in the emplacement of the gabbrodiorite and granodiorite porphyry stocks, respectively. The porphyritic granodiorite, which intruded into an older gabbrodiorite pluton (Figure 2B&C) both are associated with several post-ore dykes. The NW-SE trending post ore andesite and dioritic dykes are located in the northwest and central-eastern part of the porphyry system, cut through the granodiorite intrusion and the enclosing gabbrodiorite (Figure 1B). The ore hosting gabbrodiorite and granodiorite intruded into the andesitic to trachyandesite volcanic rocks and tuffs in the late Oligocene (Hassanpour & Moazzen, 2018).

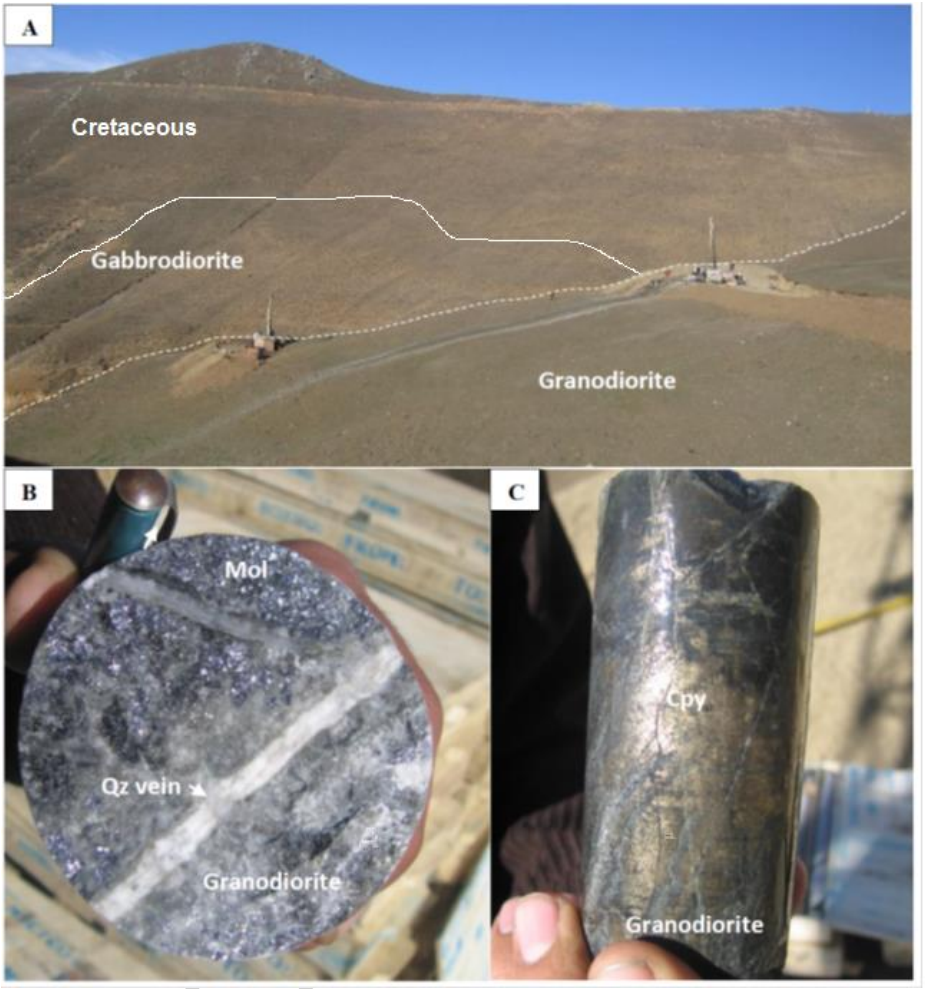

Fig. 2. Representative photographs of the field and drill cores from the Haftcheshmeh Cu-Mo porphyry system: A: Outcrop of the gabbrodiorite and granodiorite porphyry intrusions in the Haftcheshmeh area (NE landscape); B: Molybdenite and D type quartz veinlets in the granodiorite porphyry stock; C: Chalcopyrite and pyrite mineralizations in the granodiorite porphyry stock. Abbreviations: Mol=Molybdenite, Qz=Quartz (Withney & Evans, 2010).

Petrography and mineral assemblages

Petrography and allterations: In the Haftcheshmeh porphyry system, Cu-Mo mineralization occurred as various sulfide-bearing veins/veinlets and disseminated form in the main ore-forming stage (Figure 2B&C), which are associated with the potassic and propylitic and patchy phyllic alterations. Ore minerals consisted of molybdenite, pyrite, and chalcopyrite (Figure 2 B&C).

Gabbrodiorite has an ophitic (Figure 3A), and granodiorite has porphyritic textures (Figure 3B). Gabbrodiorite have plagioclase, amphibole, pyroxene and biotite as the main minerals and Granodiorite is characterized mainly by sericitized plagioclase, K-feldspar, biotite, and quartz phenocrysts. The primary biotite and K-

feldspar are altered to secondary biotite, sericite, muscovite, and opaque minerals. Both porphyry stocks are the main host of Cu-Mo mineralizations.

Based on the field investigations and petrographic observation, the hydrothermal alteration zones in the area contain dominantly potassic and propylitic alterations. The potassic alteration occurred from the surface to 700 m in depth and has an extension in the east, west, and southern parts of the area. The potassic alteration comprises secondary K-feldspar, and secondary biotite with local plagioclase, magnetite, and quartz (Figure 3 A&B). Both porphyry stocks suffered dominantly from potassic and propylitic alterations. Propylitic alteration is extended horizontally and occurs at all margins of the deposit into gabbrodiorite and Cretaceous rocks. The propylitic alteration is recognized by the presence of calcite and epidote that differentially are replaced by phenocrysts.

Mineralography: Ore minerals consisted of molybdenite, pyrite, chalcopyrite, chalcocite, bornite, covellite, and magnetite with minor amounts of tetrahedrite, galena, and sphalerite. Recently two ore minerals were observed in the southern margin of the gabbrodiorite stock, close to the very weak mineralized skarn (Figures 3C-3H). Sulfide minerals in potassic alteration zone include chalcopyrite, pyrite, galena, sphalerite, chalcocite, bornite, covellite, magnetite, and tetrahedrite (Figures 3C-3H). These minerals in this alteration zone are observed as dissemination and veins-veinlets forms.

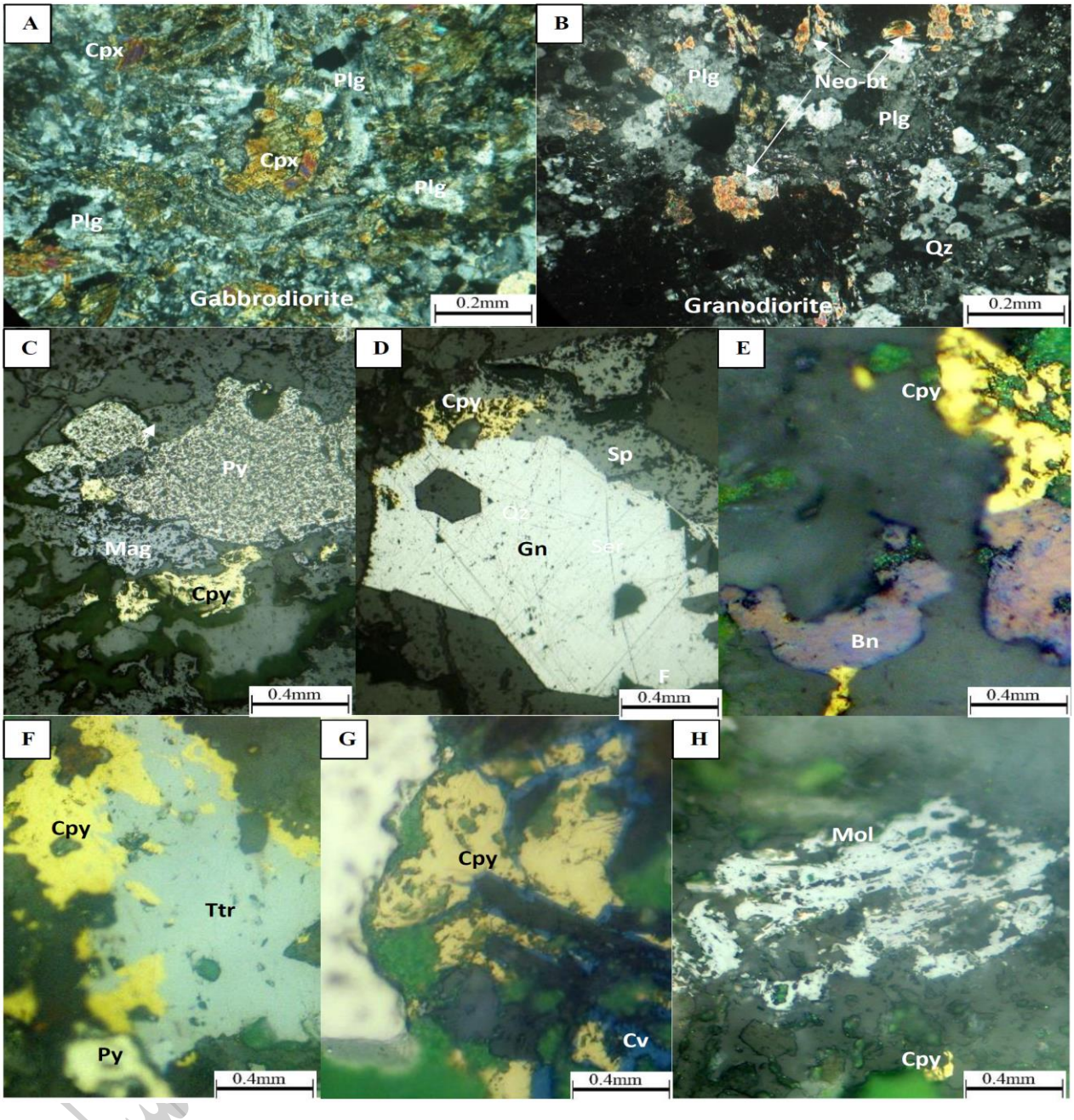

Fig. 3. Petrology and mineralogy of the Haftcheshmeh deposit: A) Phenocryst of the plagioclase and pyroxenes in an ophitic texture from fresh gabbrodiorite stock (crossed polarized transmitted light); B) Phenocryst of plagioclase, quartz, ferromagnesian (Biotite and hornblende) and opaque minerals in a granodiorite porphyry texture; C) chalcopyrite-pyrite and magnetite in granodiorite porphyry from potassic alteration zone; D) chalcopyrite, galena and sphalerite in the sample from the propylitic alteration zone. E) bornite, and chalcopyrite from potassic alteration zone in gabbrodiorite; F) chalcopyrite, pyrite, and tetrahedrite in the potassic alteration zone; G) replacement of chalcopyrite by covellite minerals in the potassic alteration zone; H) Molybdenite and chalcopyrite in the potassic alteration zone in Haftcheshmeh porphyry system. Abbreviations: Mol=Molybdenite; Cpx=Clino-Pyroxene; Plg=plagioclase; Bt=biotite; Gn=Galeana; Sp=Sphalerite; Py=pyrite; Cpy=chalcopyrite; Cv=covellite; Ttr=tetrahedrite; Bn=bornite; Mag=Magnetite. Abbreviations are from Whitney and Evans, 2010.

Haftcheshmeh magma mineral chemistry: Biotite is categorized into magmatic, reequilibrated, and hydrothermal types according to their petrographic criteria (Nachit et al., 2005). Based on the thin section examination, two different types of biotite were identified as reequilibrated and hydrothermal in Haftcheshmeh porphyry system. The reequilibrated biotites probably have a magmatic origin and texturally occur as shreddy varieties in the potassic alteration zone of the gabbrodiorite and granodiorite porphyry (Figure 4A&B; Zaheri–Abdehvand et al., 2022). Some reequilibrated biotites occurred as euhedral to subhedral phenocrysts showing ragged, splintery, or frayed features. They frequently altered to fine-grained secondary hydrothermal biotite (Figure 4C&D). They texturally occurred as aggregates of fine-grained flakes and typically had some dimensions. Amphibole grains occurred as euhedral to subhedral and had a dark core and light rim, which reflected the injection of mafic magma into the gabbrodiorite and granodiorite magma chamber (Zaheri-Abdehvand et al., 2022).

Apatite is categorized into magmatic and hydrothermal types according to their petrographic studies in the Haftcheshmeh (Figure 4E). In backscattered electron (BSE) imaging, the magmatic apatite (Ap_m) is observed as inclusions within the amphibole and, to a lesser extent, within biotite and as individual crystals in the groundmass (Figure 4F). It is euhedral to subhedral in shape and has dimensions between 30 to 50 μm. Ap_m often appears as a homogeneous crystal. The hydrothermal apatite (Ap_h) occurred as an irregular and inhomogeneous grain. Its crystals are relatively dark compared with unaltered apatites under BSE imaging (Figure 4E).

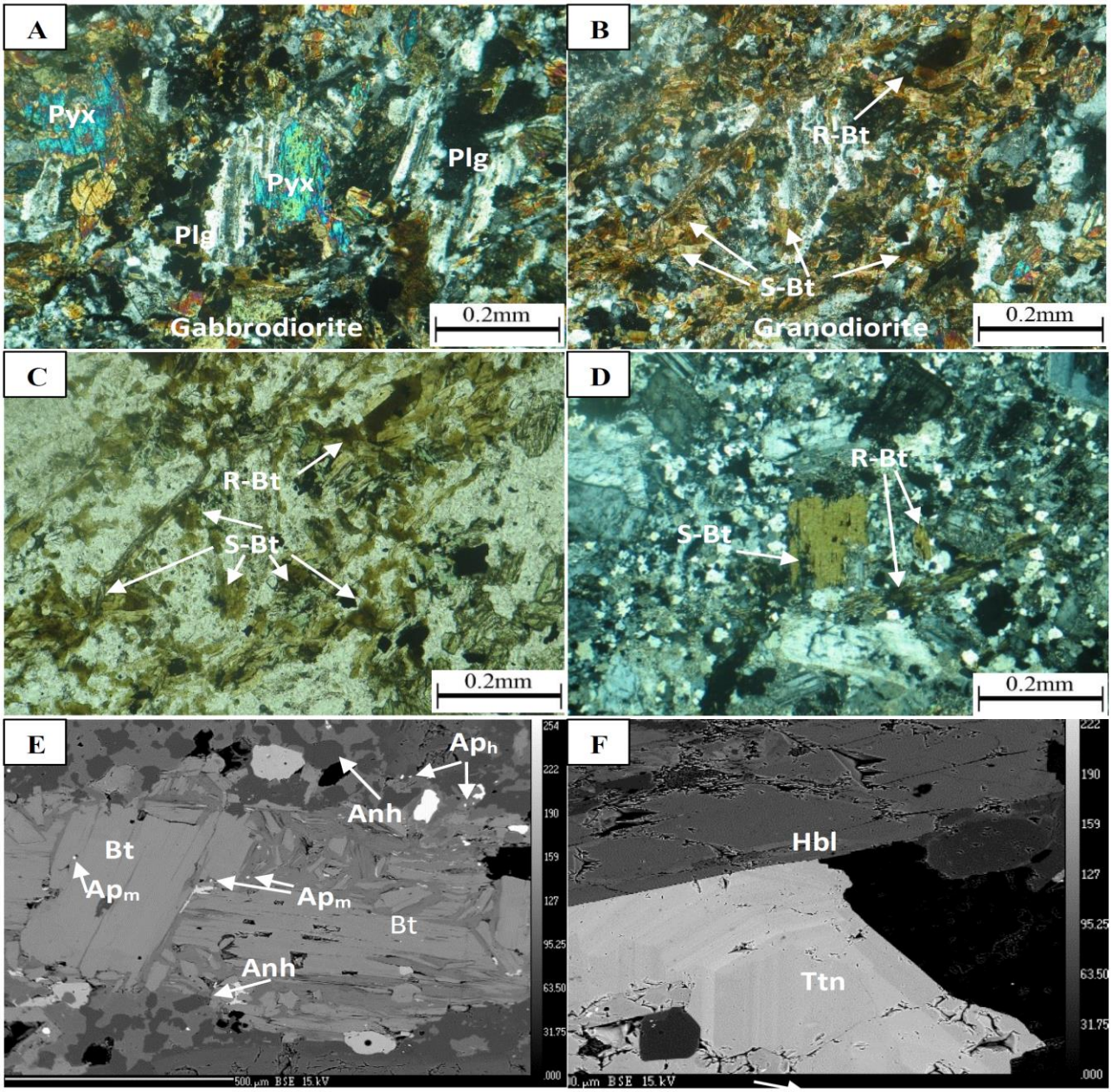

Fig. 4. Representative photomicrographs and back-scattered electron (BSE) images of biotite, amphibole, and apatite from gabbrodiorite and granodiorite porphyry of the Haftcheshmeh Cu-Mo porphyry system: A) Photomicrograph of gabbrodiorite with phenocrysts of plagioclase and pyroxene in ophitic texture (crossed polarized transmitted light); B) Reequilibrated biotite and secondary biotite in granodiorite porphyry associated with plagioclase (crossed polarized transmitted light); C) Reequilibrated biotite and secondary biotite associated with K-feldspar, quartz, and sericite in granodiorite porphyry (crossed polarized transmitted light); D) Photomicrograph of plagioclase phenocrysts replaced by hydrothermal biotite in granodiorite porphyry (crossed polarized transmitted light); E) Back-scattered electron (BSE) image of biotites and Ap grains partly as inclusions within biotite and anhydrite; F) Back-scattered electron (BSE) image of hornblende and titanite. Abbreviations: BT=biotite; R-Bt=reequilibrated biotite; S-Bt=Secondary biotite; Plg=plagioclase; Pyx=Pyroxene, Ap_h=hydrothermal apatite; Ap_{mh}=magmatic apatite; Ttn=Titanite; Anh=Anhydrite; hbl=Hornblende. Abbreviations are from Whitney and Evans, 2010.

Sampling and analytical methods

In the research, samples were taken from all type rocks of drill cores in Haftcheshmeh porphyry stocks. Polished thin sections were made from the gabbrodiorite and granodiorite porphyry system. The mineralogical and textural studies were undertaken on ten thin polished sections by optical microscope in both plane-polarized and reflected lights. Finally, five essential samples, including 13 apatites, were selected for geochemical and mineralogical analysis. Table 1 summarizes the description of the analyzed samples. Prior to analysis, 13 samples were coated with a thin film of carbon. The major and minor elements, and halogen concentrations of apatite were determined by electron microprobe analysis (EMPA) using a Camera SX100® electron microprobe at Masaryk University, Czech Republic. The lower limits of detection for major and minor elements are 0.01 wt.% and 0.001 wt.%, respectively. Standard operating conditions for Cl, F, Na, and Fe elements were an accelerating voltage of 15 kV, a beam current of 10 nA, a beam diameter of 3 μm, and counting times between 20 and 40 s. Analytical conditions for Ca, K, Si, Al, Mg, Ba, Mn, Cr, and Ti elements were an accelerating voltage of 15 kV, a beam current of 20 nA, a beam diameter of 3 μm, and a maximum total pulse integration time of 10s. Tables 1 shows the microprobe analyses of individual apatite from Haftcheshmeh rocks and their calculated chemical formulas.

Results

Apatite chemistry

Table 1 shows the major and trace element composition of apatite from Haftcheshmeh samples.

Table 1. EPMA data (in wt.% and ppm) for apatites from Haftcheshmeh porphyry deposit

Sample	Haft1	Haft2	Haft3	Haft4	Haft5	Haft6	Haft7	Haft8	Haft9	Haft10	Haft11	Haft13
AP Types	Ap_H	Ap_H	Ap_H	Ap_H	Ap_M	Ap_M	Ap_H	Ap_H	Ap_M	Ap_M	Ap_M	Ap_M
Rock type	Gbd	Gbd	Gd	Gd	Gbd	Gbd	Gd	Gd	Gd	Gd	Gbd	Gbd
Major element (wt%)												
SiO_2	0.04	0.08	0.07	0.03	0.37	0.06	0.07	0.06	0.37	0.05	0.08	0.18
Al_2O_3	0	0.01	0.01	0	0.17	0.01	0.01	0	0.02	0	0.01	0.01
MgO	0.09	0.09	0.08	0.08	0.06	0.01	0.02	0.01	0.02	0.01	0.01	0
CaO	55.13	54.95	54.52	55.45	56.017	56.06	56.68	56.16	55.52	55.28	55.42	55.13
K_2O	0.03	0.03	0.03	0.02	0.03	0.01	0	0	0	0.02	0	0
Na_2O	0.18	0.17	0.23	0.01	0.06	0.03	0.04	0.02	40	0.09	0.03	0.08
FeO	0.54	0.47	0.27	0.11	0.08	0.13	0.12	0.22	0.21	0.07	0.21	0.02
MnO	0.32	0.36	0.29	0.26	0.06	0.07	0.11	0.15	0.07	0.04	0.03	0.03
As_2O_3	0	0	0	0.021	0.045	0	0	0.007	0.073	0	0	0.004
P_2O_5	42.24	41.9	42.25	41.72	41.28	41.6	41.94	41.18	40.66	41.66	41.94	41.62
SO_2	0.07	0.09	0.13	0.09	0.09	0.03	0.08	0.14	0.17	0.02	0.06	0.11
BaO	0	0.08	0	0	0.06	0.08	0.06	0	0.04	0	0.01	0.09
SrO	0.06	0	0.06	0.07	0	0	0.08	0.01	0.05	0	0.01	0.05
Y_2O_3	0.06	0.08	0.11	0.08	0	0	0	0	0.01	0	0	0
La_2O_3	0.2	0.1	0.06	0.01	0.05	0.06	0.06	0.07	0.06	0	0	0.2
Ce_2O_3	0.3	0.17	0.18	0.12	0	0.02	0	0.02	0.09	0.03	0.04	0.12
Nd_2O_3	0.2	0.36	0	0.23	0.25	0	0	0.02	0.01	0.1	0.09	0.23
Pr_2O_3	0.18	0.18	0.14	0.04	0.16	0	0.08	0.18	0.08	0	0.02	0.09
SmO	0	0.11	0	0	0	0	0	0	0.07	0.19	0.07	0
ThO_2	0	0.04	0	0.05	0	0.12	0	0	0.05	0	0.15	0.04
Cl	0.62	0.65	0.66	0.4	0.45	0.68	0.6	0.87	0.59	0.18	0.26	0.18
Cl_m	998.4	1044.9	1053.1	643.7	720.7	1086.7	966.3	1393	947.1	292.1	423.8	293.7
F	3.15	3	3.08	3.41	3.14	2.92	2.85	2.63	2.81	3.16	3.28	3.21
F_m	2364.2	2251.6	2291.4	2615.9	2387.4	2195.4	2102.7	1950.3	2125.8	2413.9	2125.8	2500
Na	0.14	0.13	0.17	0.07	0.05	0.02	0.03	0.01	0.03	0.07	0.02	0.06
Si	0.02	0.07	0.03	0.01	0.17	0.03	0.03	0.03	0.18	0.02	0.04	0.09
Al	0	0	0	0	0.07	0.06	0.08	0	0.01	0	0.07	0.05
Mg	0.05	0.06	0.05	0.02	0.04	0	0.01	0	0.01	0.07	0.08	0
Ca	40.21	40.07	39.76	40.42	40.85	40.89	41.34	40.96	40.49	41.18	41.26	41.05
K	0.02	0.03	0.03	0.01	0.03	0	0	0	0	0	0	0
Fe	0.42	0.37	0.21	0.09	0.07	0.1	0.09	0.17	0.17	0.05	0.16	0.01
Mn	0.25	0.28	0.23	0.2	0.05	0.06	0.09	0.11	0.05	0.03	0.03	0.03
O	40.34	40.13	40.11	39.95	40.04	39.91	40.34	39.8	39.54	40.03	40.3	40.15
As	0	0	0	0.02	0.034	0	0	0	0.05	0	0	0
P	18.43	18.29	18.44	18.21	18.02	18.16	18.31	17.97	17.75	18.18	18.3	18.16

Table 1. (Continued) EPMA data (in wt. % and ppm) for apatites from the Haftcheshmeh porphyry deposit

Sample	Haft 1	Haft 2	Haft 3	Haft 4	Haft 5	Haft 6	Haft 7	Haft 8	Haft 9	Haft10	Haft11	Haft13
AP Types	Ap_H	Ap_H	Ap_H	Ap_H	Ap_M	Ap_M	Ap_H	Ap_H	Ap_M	Ap_M	Ap_M	Ap_M
Rock type	Gbd	Gbd	Gd	Gd	Gbd	Gbd	Gd	Gd	Gd	Gd	Gbd	Gbd
Major element (wt%)												
S	0.033	0.048	0.065	0.045	0.045	0.013	0.04	0.069	0.088	0.012	0.028	0.055
S_m	0.003	0.0037	0.0038	0.0039	0.004	0.0041	0.0041	0.0042	0.0043	0.0045	0.0046	0.0048
Ba	0	0.074	0	0	0.05	0.071	0.053	0	0.039	0	0.007	0.084
Sr	0.051	0	0.051	0.056	0	0	0.066	0.009	0.044	0	0.012	0.045
As	0	0	0	0.016	0.034	0	0	0.005	0.056	0	0	0.003
Y	0.049	0.06	0.085	0.066	0	0	0	0	0.005	0	0	0
La	0.175	0.086	0.048	0.007	0.044	0.051	0.05	0.057	0.051	0	0	0.137
Ce	0.255	0.144	0.151	0.102	0	0.014	0.002	0.015	0.076	0.028	0.038	0.105
Nd	0.174	0.309	0	0.202	0.214	0	0	0.017	0.007	0.083	0.079	0.2
Pr	0.151	0.152	0.12	0.032	0.133	0	0.068	0.158	0.071	0	0.015	0.081
Sm	0	0.097	0	0	0	0	0	0	0.066	0.099	0.061	0
Th	0.003	0.039	0	0.043	0	0.109	0	0	0.044	0	0.131	0.038
Total	104.54	104.05	103.28	103.39	103.49	103.03	103.97	102.91	102.18	103.12	104.04	103.68
XF	0.834	0.825	0.812	0.91	0.841	0.783	0.755	0.709	0.762	0.849	0.762	0.875
XCl	0.088	0.092	0.093	0.057	0.064	0.01	0.086	0.25	0.086	0.026	0.086	0.038
XOH	0.102	0.094	0.095	0.033	0.095	0.207	0.159	0.166	0.152	0.125	0.152	0.086
XF/XOH	8.18	8.78	8.55	27.58	8.85	3.78	4.75	4.27	5.01	6.79	5.01	10.17
XCl/XOH	0.86	0.98	0.98	1.73	0.67	0.05	0.54	1.51	0.57	0.21	0.57	0.44
XF/XCl	8.86	8.97	8.73	15.96	13.14	78.3	8.78	2.84	8.86	32.65	8.86	23.03
fO_2[2]	-9.751	-9.751	-9.751	-9.75	-9.75	-9.75	-9.75	-9.75	-9.75	-9.75	-9.75	-9.75
log(fH_2O/fHF)fluid	3.32	4.41	4.23	4.35	3.89	3.35	3.42	3.69	3.71	3.42	4.12	3.62
log(fH_2O/fHCl)fluid	1.51	1.63	1.56	1.52	1.68	1.41	1.73	1.72	1.81	1.78	1.76	1.64

X = Mole fraction;

Magmatic apatite: In the magmatic apatite magma condition is presented by CaO (9.998-10.199 apfu) and P_2O_5 (5.987-6.063 apfu P). The values of MgO and FeO range from 0 to 0.066 wt.% and from 0.018 to 0.215 wt.%, respectively, and the contents of Al_2O_3 and K_2O are 0 to 0.0126 wt.% and 0 to 0.031 wt.%, respectively.

Moreover, BaO amount is below the limits of detection to 0.094 wt.%. The analytical results show that SiO_2 and Na_2O values in Ap_H vary from 0.046 to 0.375 wt.% and from 0.011 to 0.093 wt.%, respectively. The contents of MnO in Ap_H crystals are 0.035–0.092 wt.%. The Ap grains have higher Cl contents (0.182–0.590 wt.%). The F contents are 2.811- 3.276 wt.% in apatites. The mole fractions of F, Cl, and OH (XF, XCl, and XOH) and the abundance of water (H_2O) in apatite were estimated using the model of Li and Costa (2020). Table 1 shows the XF/XOH, XCl/XOH, and XF/XCl ratios.

Hydrothermal apatite: In the hydrothermal apatite, there are CaO (9.901–10.05 apfu) Ca, where apfu refers to atomc proportion per formula unit, (apfu), and P_2O_5 (5.901–6.041 apfu P). The values of MgO and FeO range from 0.007 to 0.093 wt.% and from 0.06 to 0.542 wt.%, respectively, and the contents of Al_2O_3 and K_2O are 0 to 0.015 wt.% and 0 to 0.034 wt.%, respectively. Moreover, BaO amount is below the limits of detection to 0.083 wt.%. The analytical results show that SiO_2 and Na_2O values in Ap_H vary from 0.030 to 0.078 wt.% and from 0.019 to 0.234 wt.%, respectively. The contents of MnO in Ap_H crystals are 0.149–0.357 wt.%. The Ap grains have higher Cl contents (0.401–0.868 wt.%). The F contents are 2.635- 3.146 wt.% in apatites. The mole fractions of F, Cl, and OH (XF, XCl, and XOH) and the abundance of water (H_2O) in apatite were estimated using the model of Li and Costa (2020). Table 1 The XF/XOH, XCl/XOH, and XF/XCl ratios.

Haftcheshme apatite data in the SiO_2-MnO diagram plotted in both hydrothermal and magmatic type apatite domain in contrast to Qinling belt in China (Zhao et al., 2020; Figure 5A). Chlorine exhibits a negative correlation with F in Ap that these elements probably replace one another in the hydroxyl site and that OH is passive (Figure 5B; Azadbakht et al., 2018). In a ternary diagram of F-Cl-OH, Haftcheshme apatite data is plotted in fluorapatite with low Cl and OH contents (Figure 5C).

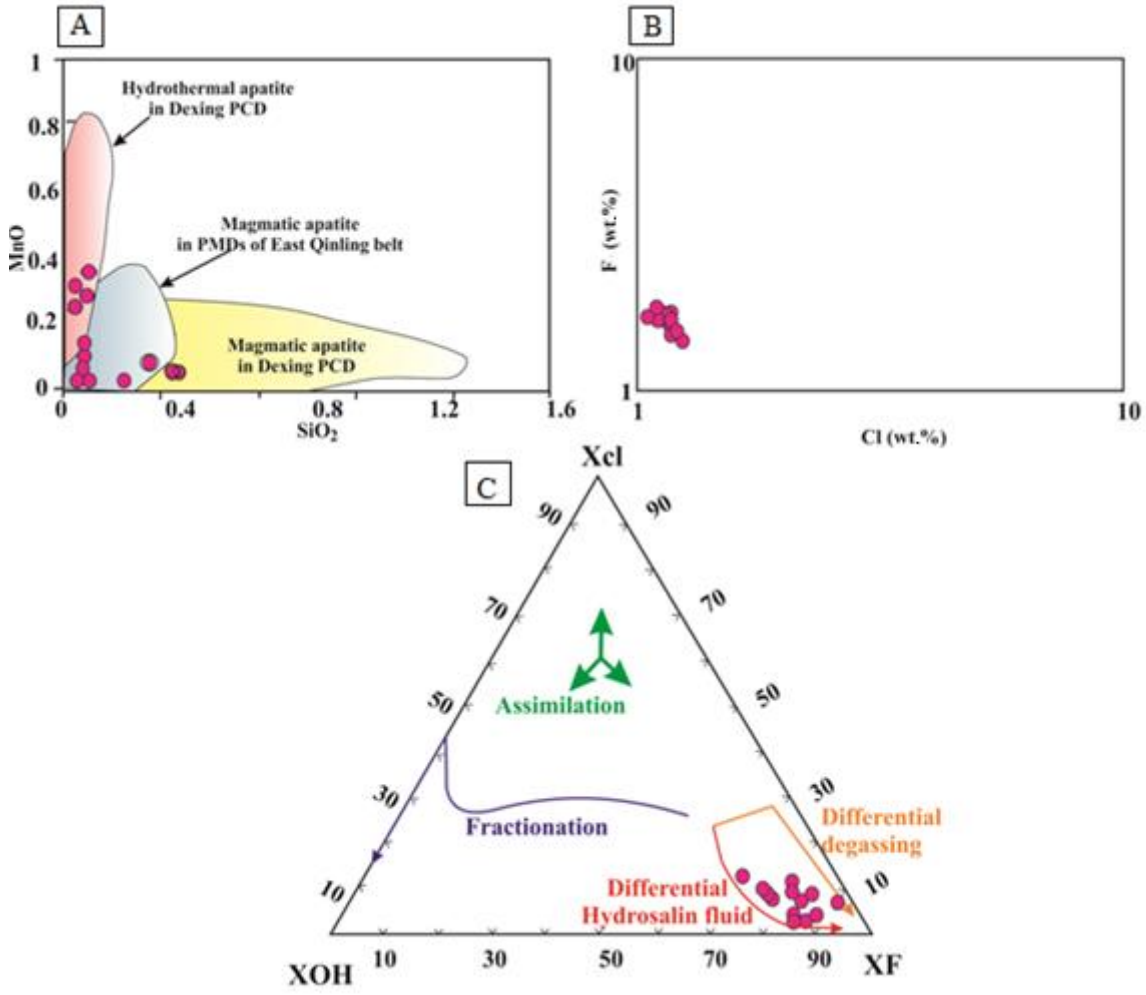

Fig. 5. Major and trace element compositions in Ap from the Haftcheshmeh porphyry deposit:(A) Plot of SiO_2 vs. MnO for apatites hosted in gabbrodiorite and granodiorite porphyry. The fields of magmatic and hydrothermal apatite in Dexing porphyry Cu deposit (PCD) and porphyry Mo deposits (PMDs) of East Qinling belt are from Zhao et al. (2020); B) Cl vs. F; C) Ternary F-Cl-OH diagram McCubbin et al. (2015). The XF-XCl-XOH are the mole fractions of each volatile component, as defined in Table 1.

Discussion

Petrogenetic implications

Crystallization conditions of apatite

The crystallization conditions of apatite is estimated by apatite saturation temperature (AST). AST can be calculated in silicate melts, assuming that the whole rock composition is equal to the initial melt composition and that apatite crystallized from the melt (Harrison & Watson, 1984). The magmatic apatite in the porphyry

systems is mostly euhedral to subhedral inclusions in minerals, implying that the apatites have crystallized close to the liquidus in these rocks. For whole-rock samples whose geochemical compositions were published by Zaheri-Abdehvand et al. (2022), Hassanpour and Moazzen (2018), the AST was calculated based on the suggested equation of Harrison and Watson (1984), as the following equation (eq. (1)):

$$D_p^{apatite/melt} = [(8400 + ((SiO_2 - 0.5)2.64 * l04))/T] - [3.1 + (12.4(SiO_2 - 0.5))] \quad (1)$$

where T is the absolute temperature (K), D_P is the distribution coefficient for phosphorus between magmatic apatite and melt, and SiO_2 is the weight fraction of silica in the melt. AST (C°) ranges from 838.41˚C to 842.58˚C (mean=841.33°C) in granodiorite porphyry (Table 2). This temperature range was confirmed by the crystallization temperatures of amphibole that recorded the range of 712°C to 1060°C (mean=886°C) and 0.96 to 0.11 Kbar (mean=0.535 Kbar) in granodiorite (Zaheri-Abdehvand et al. (2022). As a result, similar crystallization conditions (e.g., temperature, pressure, and fO_2) can be considered for apatite and amphibole in the porphyry system.

Table 2. AST(C°) samples apatites of Haftcheshme porphyr granodiorte

Sample	Haft1	Haft2	Haft3	Haft4	Haft5	Haft6	Haft7	Haft8	Haft9	Haft 10	Haft 11	Haft 12	Haft 13
AST©	842.5	842	842	843	839	842	842	842	838	842.4	842	839.7	841

Metallogenic implications

The redox state of the parental magma

Studies on porphyry systems show that most porphyry Cu (Au-Mo) deposits formed from oxidized magmas with high oxygen fugacity (Sun et al., 2015). Therefore, the oxidized magmas are favorable for porphyry mineralization Zaheri-Abdehvand et al. (2022) believed in the Al-amphibole, and biotite a ranges of calculated temperatures of saturation temperature (712°C to 1060°C) and (695°C to 720°C), respectively, pressures (0.11 to 0.96 Kbar, corresponding to depths of 1.3 to 2.9 km based on amphibole barometry) and H_2O_{melt} content (>3 wt.%), suggesting a hydrous calc-alkaline magma generated from a deep magmatic source.

The abundances of redox-sensitive elements, such as Mn, Ce, Eu, and S in apatite, can be used as indicators for determining a magma's oxidation state (Miles et al., 2014). Recently, it was proposed that Mn contents in apatites from a range of intermediate to silicic igneous rocks may be useful in indicating fO_2. The oxygen fugacity of apatites in Hafcheshmeh can be calculated based on the following Mn as an oxy barometer and redox proxy expression of Miles et al. (2014):

$\log fO_2$= -0.0022 (±0.0003) Mn (ppm) -9.75 (±0.46) (2)

The calculated oxygen fugacity (fO_2) for the porphyry system ranges from -9.750 to -9.751 (Miles et al., 2014). As sulfur substitutes into apatite as S^{6+}, several substitution mechanisms control the incorporation of sulfur in apatite (Parat et al., 2011). Sulfur is the most important geo solvent that controls the behavior of chalcophile elements such as Cu, Au, and Mo (Sun et al., 2015). These elements act as incompatible elements in sulfide undersaturated magmas, leading to high chalcophile element concentrations in derivative magmas (Sun et al., 2015). The high amounts of S in apatite are associated with high $fO2$, indicative of oxidized magmas. One of the important methods of showing oxygen fugacity based on the chemical compositions of apatite is Log fO2 vs. T(C°) diagram (Sun et al., 2015). The T(°C) vs. log $fO2$ diagram is suggested to display the oxygen fugacities of oxidized porphyry deposits (Sun et al., 2015). According to the diagram, apatite from Haftcheshmeh porphyry Cu-Au deposit fall in I-type oxidized magma domain (Figure 6). Therefore, the intrusion of Haftcheshmeh was an oxidized I-type magma system with high $fO2$ (Figure 6). Oxygen fugacity obtained from the amphibole-only thermometer suggests that the gabbrodiorite and granodiorite intrusions have crystallized from oxidized (NNO + 1.82 and NNO + 2.92) magmas during amphibole crystallization (Zaheri-Abdehvand et al., 2022).

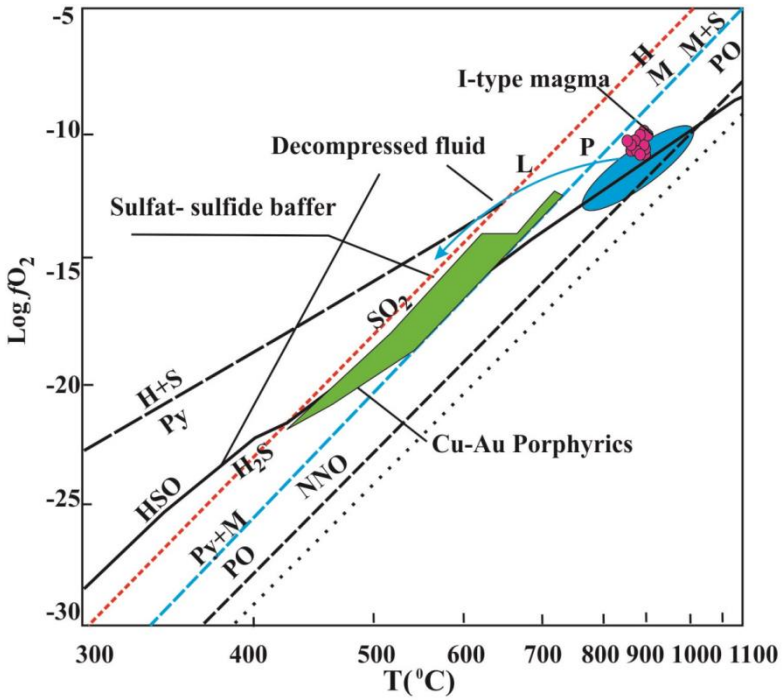

Figure 6. Compositions of apatites from the Haftcheshmeh deposit on Oxygen T(°C) vs. log fO_2 diagram for the oxygen fugacities of oxidized porphyry deposits (Sun et al., 2015); Abbreviations: MH-Magnetite-Hematite buffer curve; NNO-Nickel-Nickel Oxide buffer curve; FMQ-Fayalite-Magnetite-Quartz buffer curve.

Implication of halogen elements

Halogen fugacity of associated fluids from apatite chemistry

It seems that diffusion of the volatiles within apatite has occurred during the protracted cooling process of the igneous rocks (Zhao et al., 2020). The halogen fugacity ratios were obtained from a model presented by Piccoli et al. (1999). This model is based on estimating the HCl and HF fugacity in the magmatic volatile phase (MVP) from concentrations of Cl and F in apatite chemistry:

$$\log (f\mathrm{H_2O}/f\mathrm{HCl})^{\mathrm{fluid}} = \log (\mathrm{X(Hap)}/\mathrm{X(Clap)}) + 0.04661 + (2535.8 - 0.0303*(\mathrm{P(bar)} - 1))/\mathrm{T(K)} \quad (3)$$

$$\log (f\mathrm{H_2O}/f\mathrm{HF})^{\mathrm{fluid}} = \log (\mathrm{X(Hap)}/\mathrm{X(Fap)}) + 0.18219 + (5301.1 - 0.00360*(\mathrm{P(bar)} - 1))/\mathrm{T(K)} \quad (4)$$

where P is in a bar, T is the temperature (K), and X(Clap), X(Fap), and X(Hap) are mole fractions of chlorapatite, fluorapatite, and hydroxylapatite. Piccoli et al. (1999) suggested that pressure can be estimated by amphibole geobarometry in the calculations. The values of log ($f\mathrm{H_2O}$)/(fHCl) and log ($f\mathrm{H_2O}$)/(fHF) ratios were calculated in fluids related to apatite (Table 1). We considered the calculated AST (838.41˚C to 842.58˚C) and the amphibole crystallization pressure (0.11-0.96 Kbar) as T and P in these equations from Zaheri-Abdehvand et al. (2019). The concentrations of the log ($f\mathrm{H_2O}$)/ (fHCl) in fluids of apatite are between 1.41 and 1.73 (mean=1.57). The contents of log ($f\mathrm{H_2O}$/fHF) in fluids of apatite range from 3.32 to 4.41 (mean=3.86), which imply apatites equilibrated with F-rich fluids (Table 1).

The estimation of volatile content in the melt from apatite composition

The thermodynamic studies propose models to calculate the abundances of water in the melt using concentrations of volatiles (F, Cl, $\mathrm{H_2O}$???) in apatite and the exchange coefficients (KD) for OH-Cl, OH-F, and Cl-F between apatite and melt (Li & Costa, 2020; Table 1). The known concentrations of one of three constituents (F or Cl or $\mathrm{H_2O}$) in the melt is essential to determine the volatile and water contents of the magma. In this research, we have no information about the F-Cl-$\mathrm{H_2O}$ amounts of the melt. To acquire the F and Cl concentrations of the melt that equilibrated with the Haftcheshmeh apatites, we used experimental data provided by Webster et al. (2009) and Doherty et al. (2014) to estimate the partitioning of F and Cl between apatite, melt (A/CNK of 0.94-1.11 and N/NK of 0.62-0.79) (Table 1), and aqueous fluid at 53 and 192 MPa and 914-928°C. The molar A/CNK and N/NK of the melts from Haftcheshmeh whole-rock compositions range from 0.82 to 1.24 and 0.51 to 0.69, respectively (Hassanpour & Moazzen, 2018) and are almost consistent with experimental data. The apatite-melt partitioning of F can be calculated by Equation 5 (Webster et al., 2009):

$$\mathrm{F\ (wt.\%\ in\ melt)} = [(\mathrm{XF\ in\ Apatite} - 0.12]/3.02 \quad (5)$$

where XF is the molar F concentration in the apatite, based on the results, the apatite in the porphyry deposit indicates F melt values ranging from 0.70 to 0.91 wt.% (mean=0.8 wt.%). The concentrations of Cl melt can be determined based on the apatite-melt Cl partitioning equation of Bao et al. (2016), which uses experimental data from Webster et al. (2009) and Doherty et al. (2014) (Equation 6):

Cl (wt.% in melt)= (Cl wt.% in apatite)*0.16052 (6)

The equation involves a simple weight-based Nernstian partition coefficient approach (Bao et al., 2016). In the study, according to the theoretical estimate, the melt equilibrated with apatite in the porphyry deposit contained 0.253-0.01 wt.% Cl (mean=0.12 wt.%). The partition coefficient of S between apatites and the melt is a function of temperature, fO_2, and the S concentration in the melt (Peng et al., 1997). The concentration of S increases with decreasing temperature, increasing fO_2, and increasing S content in the melt (Parat et al., 2011). Oxygen fugacity deduced from apatite indicates that the Haftcheshmeh ore-forming magmas have a high fO_2 (Figure 6). The S melt concentrations can be estimated based on the experimental relationship for sulfur between apatite and melt of Parat et al. (2011) (Equation. 7):

$S_{apatite}$ (wt.%) = 0.0629 × ln S_{melt} (wt.%) + 0.4513 (r^2 = 0.68) (7)

Therefore, S contents in apatite are associated with S abundance in the melt with a high fO_2. Using the equation of Parat et al. (2011), we obtain S melt amounts ranging from 0.003 to 0.0048 wt.% (mean=0.0039 wt.%). According to the S in the melt (wt.%) vs. S (wt.%) in apatite diagram by Parat et al. (2011) (Figure 7A), the S content in apatites of Haftcheshmeh increases with increasing S content in the melt. Another proposed method for the calculation of S content in the melt is an apatite-melt partition coefficient formula that is controlled by temperature only (Peng et al., 1997), (Equation 8):

ln (S_{Ap}/S_{melt} (wt%)) = 21130/T (in Kelvin) -16.2 (8)

Using Equation 8, S melt values range from 1.68 to 1.74 wt.% (mean=1.71 wt.%) for the porphyry deposit, which indicates increasing S melt content at lower temperatures. Moreover, on the basis of the diagrams of Parat et al. (2011), the Cl in the melt (wt.%) vs. Cl in apatite (wt.%), and the F in the melt (wt.%) vs. F in apatite (wt.%) plotted in diagrams (Figure 7B&C). According to this diagrams, content of F and Cl in the melt was much more than the apatites.

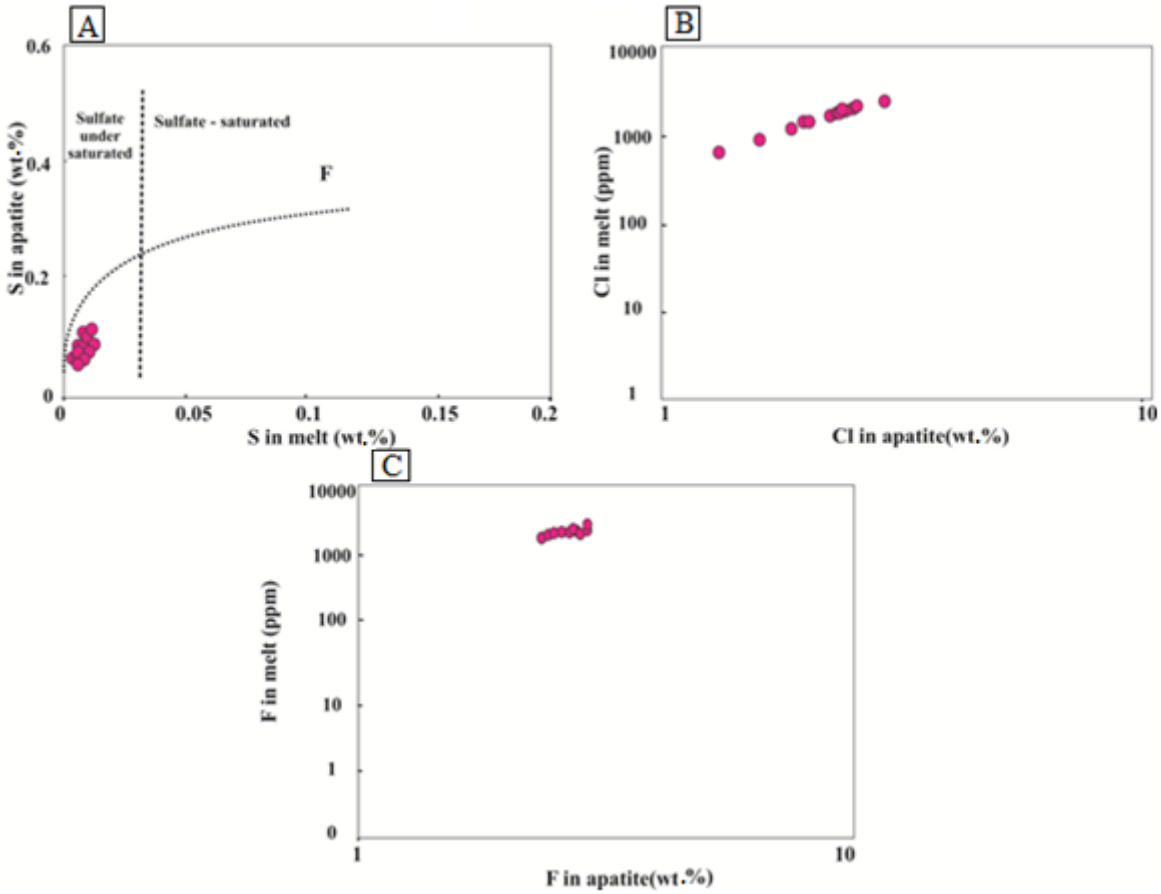

Fig. 7. Sulfur, Cl, and F concentrations in the melt and apatite in the Haftcheshmeh deposit: A) S in the melt (wt.%) vs. S in apatite (wt.%) diagram (Parat et al., 2011); B) the calculated Cl (ppm) content of the melt and Cl (wt.%) in the same apatite grains; C) the calculated F (ppm) content of the melt and F (wt.%) in the same apatite grains. Abbreviations: Ap_m-magmatic apatite.

Thermodynamic modeling of apatite volatile elements evolution

Volatile elements (e.g., F, Cl, S, and H_2O) in silicate melts have a crucial impact on the magmatic evolution and eruption of volcanoes (Li & Costa, 2020). The evolution of magmatic volatiles in a vapor-undersaturated melt controls the depths of magma storage and source melt composition (Li et al., 2020). Moreover, these elements with the transportation and deposition of metals can determine the formation style of porphyry Cu systems (Li et al., 2020). Measuring volatiles is difficult because they are not always available in most plutonic-related magmatic-hydrothermal deposits (Zhao et al., 2020). The apatite crystal structure is occupied by numerous volatile elements Cl, F, H_2O (OH), S, and CO_2 (Li & Costa, 2020). Furthermore, apatite occurs as inclusions in other igneous minerals or as fine-grained crystals in the groundmass, making it a popular tool for recording volatile budgets in melts and their variations in ore-forming magmas related to porphyry Cu deposits

(Li & Costa, 2020; Li et al., 2020). Recently, thermodynamic models have been suggested based on the partition behavior of F-Cl-OH between apatite and silicate melts (Li & Costa, 2020; Popa et al., 2021), which considers the ideal behavior of F, Cl, and OH in apatite in most of these models (Popa et al., 2021). In this study, in order to understand the behavior of F, Cl, and OH between apatite and their coexisting melt, as well as to estimate melt contents of volatiles, we applied thermodynamic modeling of apatite compositions based on the method proposed by Li and Costa (2020). Because this thermodynamic model is built based on the non-ideal mixing properties in apatite solution, the interaction parameters (W^G) and Gibbs free energies were calculated by regressing experimental data from the literature. Li and Costa (2020) proposed equations for calculating the exchange coefficients of F, Cl, and OH (K_D) between apatite and silicate melts as follows (Equations 9, 10, 11):

$$\ln\left(K_D{}^{Ap-melt}{}_{OH-Cl}\right) = -\frac{1}{RT}\times\left[72900(\pm2900) - 34(\pm0.3)\times T - 1000\times\left(5(\pm2)\times\left(X^{Ap}{}_{Cl} - X^{Ap}{}_{OH}\right) - 10(\pm8)\times X^{Ap}{}_{F}\right)\right] \quad (9)$$

$$\ln\left(K_D{}^{Ap-melt}{}_{OH-F}\right) = -\frac{1}{RT}\times\left[94600(\pm5600) - 40(\pm0.1)\times T - 1000\times\left(7(\pm4)\times\left(X^{Ap}{}_{F} - X^{Ap}{}_{OH}\right) - 11(\pm7)\times X^{Ap}{}_{Cl}\right)\right] \quad (10)$$

$$\ln\left(K_D{}^{Ap-melt}{}_{Cl-F}\right) = -\frac{1}{RT}\times\left[21700(\pm6300) - 6(\pm0.3)\times T - 1000\times\left(16(\pm6)\times\left(X^{Ap}{}_{F} - X^{Ap}{}_{Cl}\right) - 2(\pm5)\times X^{Ap}{}_{OH}\right)\right] \quad (11)$$

where temperature (T) is in Kelvin, apatite compositions are expressed in measured mole fractions of Cl, F, and OH in apatite. ($X^{Ap}{}_i$), and R is the universal gas constant. In addition, the activity coefficients of F, Cl, and OH in apatite ($\boldsymbol{\gamma}^{Ap}{}_i$) and the melt H_2O contents are calculated by this model. For calculating H_2O concentrations, a melt with 900°-950°C and 200-500 Mpa charachteristics was used. Thus, we estimated the melt H_2O concentrations, the activity coefficients of F, Cl, and OH in apatite ($\boldsymbol{\gamma}^{Ap}{}_i$), the exchange coefficients of F, Cl, and OH (K_D) between apatite and silicate melts, the melt OH contents, and the mole fractions of F, Cl, and OH apatite in equilibrium with the melt composition using this model. Based on the results, the apatite in gabbrodiorite and granodiorite porphyry indicates F melt values ranging from 2635 to 3411 ppm (mean=3023 ppm) and Cl melt concentrations range from 182 to 677 ppm (mean=429 ppm). The strong correlation between Cl contents in apatite and the calculated amount of Cl in the coexisting melt (R^2=0.97) suggests that Cl values of apatite are a true indicator for the measurement of melt Cl concentration in samples (Figure 7B). Furthermore, the positive correlation between estimated contents of F for the coexisting melt with the F amounts in apatite (R^2=0.99) indicates that F concentrations in apatite are used to estimate melt F content, considering F-Cl-OH exchange reactions (Figure 7C). Contents of XF/XCl and XCl/XOH in Haftcheshmeh porphyry deposit are compared with the values of these ratios in intrusions of Duolong Cu-Au porphyry deposit (Figure 8). All of XF/XCl and XCl/XOH ratios in apatites of Haftcheshmeh indicate a trend of magmatic and fluid exsolution evolution, suggesting trend of volatile-undersaturated crystallization that means they crystallized from the magma before vapor saturation (Figure 8) (Li et al., 2020). Thus, these apatite grains

crystallized from a gabbrodiorite and granodiorite melt at high temperatures. They show a notable similarity between apatite grains in the gabbrodiorite and granodiorite porphyry of Haftcheshmeh and the apatite of the diorite intrusion of Dubuza. Therefore, it seems that volatile elements variations in magmatic apatites of the porphyry could reflect apatite crystallization from volatile-undersaturated melts and magmatic evolution in ore-forming magmas.

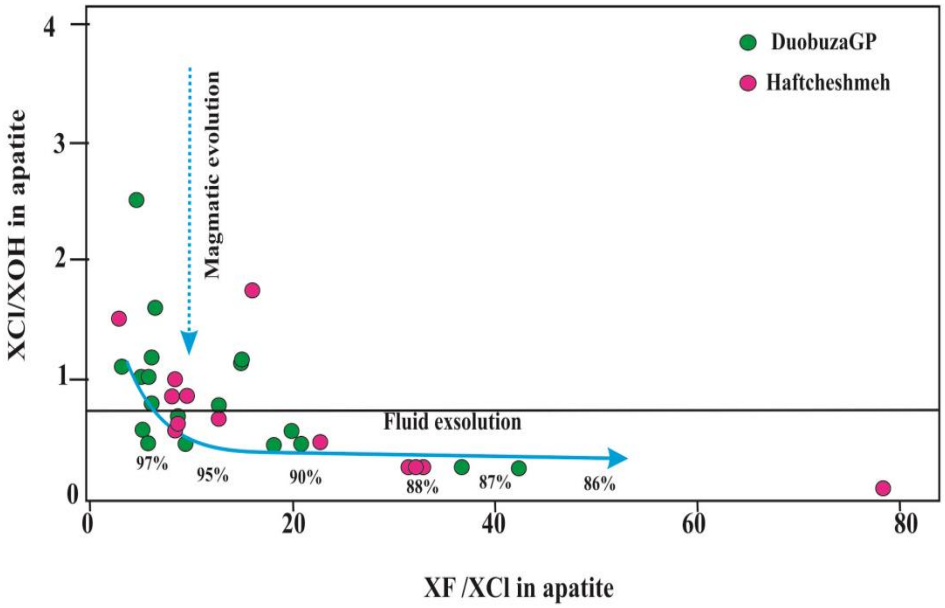

Fig. 8. Comparison of changes in volatile apatite elements from the porphyry of Haftcheshmeh with changes in apatite volatile elements from intrusions of Duolong porphyry Cu-Au deposit. These figures show compositional changes in volatile apatite elements during the evolution from volatile-undersaturated to volatile-saturated magma. XF/XCl vs. XCl/XOH in apatite; Blue solid curves in diagram calculated by the Rayleigh fractionation model represent the variation of volatile elements in apatite during fluid exsolution. Data from apatite inclusions in biotite phenocrysts from ore-bearing granodiorite porphyries of Duolong porphyry Cu-Au deposit are from Li et al. (2020). Abbreviations: GP=granodiorite porphyry.

The formation model of Haftcheshmeh Cu-Mo porphyry system

Figure 9 shows the magmatic evolution model for Haftcheshmeh Cu-Mo porphyry system. Hydrothermal apatite crystallization in the system began in ~840°C (Figure 9). Presence of zonal amphibole in both intrusions show the injection of mafic magma into the magma chamber and mixing occurred through multiple crystallization stages of amphiboles at a depth of ~8-11 km (712- 1060°C) (Zaheri-Abdehvand et al., 2022; Figure 9). The later magma with biotites probably has crystallized in a lower depth and temperatures (~8 km

and ~810˚C; Zaheri-Abdehvand et al., 2022; Figure 9), then mixed magma ascended and intruded into the country rocks. By using existing empirical equations as a mineral thermometer proved, such mineral crystallizations show that the temperatures of the apatite saturation temperature (~840°C) are among amphibole and biotite (Zaheri-Abdehvand et al., 2022).

A hydrous mafic oxidized magma ascended from a deeper reservoir into the gabbrodiorite and granodiorite magma chamber at a depth of ~7 to ~10 km (Hassanpour & Moazzen, 2018; Figure 9). Consequently, the hydrous mafic magma from a magma source was injected into the gabbrodiorite and granodiorite magma chamber, and resulted in an extensive magma mixture. Then, hydrothermal crystallization of apatite continued and caused Haftcheshmeh porphyry system that is associated to ore forming fluid exsolutions (Hassanpour & Moazzen, 2018; Figure 9). Consequently, crystallization of apatite accompanied by high fO_2, high water content, and metal contents in the mafic magma play a vital role in the formation of Haftcheshmeh porphyry system.

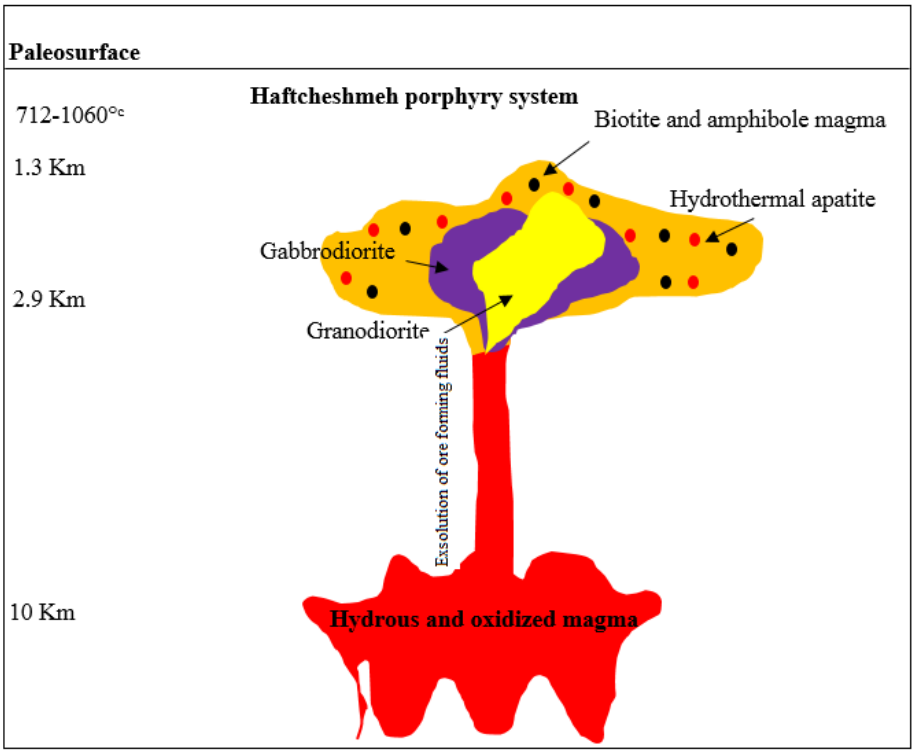

Fig. 9. Schematic model illustrating mineral crystallization sequences in Haftcheshmeh evolved mafic to felsic magma chamber: Hydrothermal apatite grains crystallized in an oxidized and hydrous mafic magma from a deeper magma reservoir in~840°C. Schematic amphibole, and biotite drawn data in the model is from Zaheri-Abdehvand et al. (2022).

Tectono-magmatic attributes

The chemical composition of apatite, biotite, and amphiboles are used as proxy to determine the tectono-magmatic setting of host igneous rocks (Hammarstrom & Zen, 1986; Li et al., 2020; Parat et al., 011). Based on Hassanpour and Moazzen (2018) and Zaheri-Abdehvand et al. (2022), the tectono-magmatic setting of Haftcheshmeh porphyry indicated a porphyry system calk-alkaline in the subduction zone that formed by a crust-mantle mixed source and high water content of the parental magma (>3 wt% H2O).

The intrusions of Haftcheshmeh represent I-type granites. The porphyry system has located in the crust-mantle mixed source domain (Zaheri-–Abdehvand et al., 2022). The parental magma of intrusions in Haftcheshmeh porphyry deposit were generated by the mixing of the subduction mantle-derived and crust-derived magma in the magma chamber (Hassanpour & Moazzen, 2018; Zaheri-Abdehvand et al., 2022).

Based on the model, a hydrous mafic magma ascended from a deeper part into the magma chamber at depth of 7 to 10 km. Then, at first, gabbrodiorite body was intruded and gabbrodioritic magma revolved to granodiorite and formed another porphyry system in upper part of the crust at approximately 2.9 to 1.3 km depths. Eventually, The Haftcheshmeh porphyry system formed by hydrothermal process and caused and associated to ore forming fluid exsolutions.

Conclusion

Based on the results and discussions, the following conclusions are drawn:

1. The apatite saturation temperature shows ranges of calculated temperatures (839°C to 842°C), pressures (0.11 to 0.96 Kbar), corresponding to depths of 6 to 10 km, suggesting the presence of a deep magmatic source for Haftcheshmeh;

2. The apatites fO_2 range from -9.750 to -9.751. All analyzed apatites show that Haftcheshmeh ore forming magmas are oxidized I-type magma. The contents of the log (fH_2O/fHF) and log (fH_2O)/ ($fHCl$) ratios of fluids equilibrated with apatites range from 3.32 to 4.46 and from 1.41 to 1.73, respectively, which imply apatites equilibrated with F rich fluids;

3. All the XF/XCl and XCl/XOH ratios in the apatite of Haftcheshmeh indicate a trend of magmatic evolution, suggesting a trend of volatile-undersaturated crystallization, which means that they crystallized in the hydrothermal fluid by differential degassing and differential hydrosol in a fluid of the vapor saturation. Moreover, the trend of volatile element variations displays that primary volatile exsolution probably occurred at temperatures between 839°C and 842°C;

4. The injection of oxidized and hydrous mafic magma from a deeper magma reservoir may result in extensive magma mixing and continuous fractional crystallization of apatite in the evolved gabbrodiorite and

granodiorite magma chamber, leading to the formation of Haftcheshmeh deposit with the exsolution of ore-forming fluids.

References

Adeli, Z., 2012. Mineralogy, geochemistry, genesis, and modeling of the Haftcheshmeh deposit, East Azerbaijan, Iran. PhD Thesis, Islamic Azad University of Tehran, Science and Research Brunch, Tehran, Iran. 275 p (in Persian with English abstract)

Azadbakht, Z., Lentz, D.R., McFarlane, C.R., 2018. Apatite chemical compositions from Acadian-related granitoids of New Brunswick, Canada: implications for petrogenesis and metallogenesis. Minerals 8 (12): 598. https://doi.org/10.3390/min8120598

Bao, B., Webster, J.D., Zhang, D.H., Goldoff, B.A., Zhang, R.Z., 2016. Compositions of biotite, amphibole, apatite and silicate melt inclusions from the Tongchang mine, Dexing porphyry deposit, SE China: Implications for the behavior of halogens in mineralized porphyry systems. Ore Geology Reviews, . 79, 443-462. https://doi.org/10.1016/j.oregeorev.2016.05.024

Doherty, A.L., Webster, J.D., Goldoff, B.A., Piccoli, P.M., 2014. Partitioning behavior of chlorine and fluorine in felsic melt-fluid (s)-apatite systems at 50 MPa and 850-950 °C. Chemical Geology, 384, 94-111. https://doi.org/10.1016/j.chemgeo.2014.06.023

Hammarstrom, J.M, Zen, E., 1986. Aluminum-in-hornblende: an empirical igneous geobarometer. American Mineralogist 71(11-12), 1297-1313. Retrieved July 17, 2023 from https://pubs.geoscienceworld.org/msa/ammin/article-abstract/71/11-12/1297/104900/Aluminum-in-hornblende-An-empirical-igneous

Harrison, T.M., Watson, E.B., 1984. The behavior of apatite during crustal anatexis: equilibrium and kinetic considerations. Geochimica et Cosmochimica Acta 48(7): 1467-1477. https://doi.org/10.1016/0016-7037(84)90403-4

Hassanpour, Sh., 2010. Metallogeny and mineralization of Cu-Au in Arasbaran zone (NW Iran) - Unpublished PhD. Thesis, Shahid Beheshti University, Tehran, Iran. 231 p

Hassanpour, S., Alirezaei, S., Selby, D., Sergeev, S., 2015. SHRIMP zircon U–Pb and biotite and hornblende Ar–Ar geochronology of Sungun, Haftcheshmeh, Kighal, and Niaz porphyry Cu–Mo

systems: evidence for an early Miocene porphyry-style mineralization in northwest Iran International Journal of Earth Sciences, 104, 45–59.https://doi.org/10.1007/s00531-014-1071-0

Hassanpour, S., and Moazzen, M., 2018, Geochronological Constraints on the Haftcheshmeh Porphyry Cu-Mo-Au, Ore Deposit, Central Qaradagh Batholith, Arasbaran Metallogenic Belt, Northwest Iran, ACTA GEOLOGICA SINICA, Vol. 91 No. 6 pp.2109–2125, https://doi.org/10.1111/1755-6724.13452

Li, J.X., Li, G.M., Evans, N.J., Zhao, J.X., Qin, K.Z., Xie, J., 2020. Primary fluid exsolution in porphyry copper systems: evidence from magmatic apatite and anhydrite inclusions in zircon. Mineralium Deposita 56 (2), 407-415. https://doi.org/10.1007/s00126-020-01013-4

Li, W., Costa, F., 2020. A thermodynamic model for F-Cl-OH partitioning between silicate melts and apatite including non-ideal mixing with application to constraining melt volatile budgets. Geochimica et Cosmochimica Acta, 269, 203-222. https://doi.org/10.1016/j.gca.2019.10.035

McCubbin, F.M., Vander Kaaden, K.E., Tartese, R., Boyce, J.W., Mikhail, S., Whitson, E.S., Bell, A.S., Anand, M., Franchi, I.A., Wang, J., Hauri, E.H., 2015. Experimental investigation of F, Cl, and OH partitioning between apatite and Fe-rich basaltic melt at 1.0-1.2 GPa and 950-1000°C. American Mineralogist, 100(8-9): 1790-1802. https://doi.org/10.2138/am-2015-5233

Miles, A., Graham, C., Hawkesworth, C., Gillespie, M., Hinton, R., Bromiley, G., 2014. Apatite: a new redox proxy for silicic magmas? Geochimica et Cosmochimica Acta, 132, 101-119. https://doi.org/10.1016/j.gca.2014.01.040

Nabavi, H., 1976. An introduction to the geology of Iran: Tehran, Geological Survey of Iran, 109 p. (in Persian).

Nachit, H., Ibhi, A.., Abia, El-H., Ben Ohoud, M., 2005. Discrimination between primary magmatic biotites, reequilibrated biotites, and neoformed biotites. Comptes Rendus Geoscience 337 (16): 1415-1420. https://doi.org/10.1016/j.crte.2005.09.002

Pan, T., Yuchuan, C., Juxing, T., Ying, W., Wenbao, Z., Qiufeng, L., Bin, L., Chunneng, W., 2019. Advances in Research of Mineral Chemistry of Magmatic and Hydrothermal Biotites. Acta Geologica Sinica (English Edition) 93(6), 1947-1966. https://doi.org/10.1111/1755-6724.14395

Parat, F., Holtz, F., Klügel, A., 2011. S-rich apatite-hosted glass inclusions in xenoliths from La Palma: constraints on the volatile partitioning in evolved alkaline magmas. Contributions to Mineralogy and Petrology,162, 463-478. https://doi.org/10.1007/s00410-011-0606-7

Peng, G., Luhr, J.F., McGee, J.J., 1997. Factors controlling sulfur concentrations in volcanic apatite. American Mineralogist 8(11-12): 1210-1224. https://doi.org/10.2138/am-1997-11-1217

Piccoli, P., Candela, P., Williams, T., 1999. Estimation of aqueous HCl and Cl concentrations in felsic systems. Lithos 46(3): 591-604. https://doi.org/10.1016/S0024-4937(98)00084-X

Piccoli, P.M. and Candela, P., 2002. Apatite in Igneous Systems. In: J.K. Matthew, J. Rakovan and J.M. Hughes (Editors), Phosphates, De Gruyter, pp, 55-292. https://doi.org/10.1515/9781501509636-009

Popa, R.-G., Tollan, P., Bachmann, O., Schenker, V., Ellis, B., Allaz, J.M., 2021. Water exsolution in the magma chamber favors effusive eruptions: application of Cl-F partitioning behavior at the Nisyros-Yali volcanic area. Chemical Geology, 570, 120170. https://doi.org/10.1016/j.chemgeo.2021.120170

Ridolfi, F and Renzulli, A., 2012. Calcic amphiboles in calcalkaline and alkaline magmas: thermobarometric and chemometric empirical equations valid up to 1130 oC and 2.2 GPa. Contributions to Mineralogy and Petrology 163, 877-895. https://doi.org/10.1007/s00410-011-0704-6

Sun, W.D., Huang, R.F., Li, H., Hu, Y.B., Zhang, C.C., Sun, S.J., Zhang, L.P., Ding, X., Li, CY., Zartman, R.E., Ling, M.X., 2015. Porphyry deposits and oxidized magmas. Ore Geology Reviews, 65(part 1): 97-131. https://doi.org/10.1016/j.oregeorev.2014.09.004

Webster, J., Thomas, R., Foerster, H.J., Seltmann, R., Tappen, C., 2004. Geochemical evolution of halogen-enriched granite magmas and mineralizing fluids of the Zinnwald tin-tungsten mining district, Erzgebirge, Germany. Mineralium Deposita, 39(4), 452-472. https://doi.org/10.1007/S00126-004-0423-2

Webster, J.D., Tappen, C.M., Mandeville, C.W., 2009. Partitioning behavior of chlorine and fluorine in the system apatite-melt-fluid. II: felsic silicate systems at 200 MPa. Geochimica et Cosmochimica Acta, 73(3): 559-581. https://doi.org/10.1016/j.gca.2008.10.034

Withney, D.L., and Evans, B.W., 2010. Abbreviations for names of rock-forming minerals. American Mineralogist, Volume 95(1): pages 185–187. https://doi.org/10.2138/am.2010.3371

Zaheri–Abdehvand, N., Hassanpour, S., Rasa, I., Rajabpour, S., 2022, Silicates chemistry as indicators of physicochemical and geothermometry conditions on porphyry ore system: A case study of the Haftcheshmeh Cu–Mo deposit, NW Iran, Ore Geology Reviews, 142: 104716. https://doi.org/10.1016/j.oregeorev.2022.104716

Zhao, J., Qin, K., Evans, N.J., Li, G., Shi, R., 2020. Volatile components and magma-metal sources at the Sharang porphyry Mo deposit, Tibet. Ore Geology Reviews, 126: 103779. https://doi.org/10.1016/j.oregeorev.2020.103779

Zhong, S., Feng, C., Seltmann, R., Li, D., Dai, Z., 2018. Geochemical contrasts between Late Triassic ore-bearing and barren intrusions in the Weibao Cu–Pb–Zn deposit, East Kunlun Mountains, NW China: constraints from accessory minerals (zircon and apatite). Mineralium Deposita, 53 (6), 855-870. https://doi.org/10.1007/s00126-017-0787-8

Zhong, S., Li, S., Feng C, Liu, Y., Santosh, M., He, S., Qu, H., Liu, G., Seltmann, R., Lai, Z., Wang, X., Song, Y., Zhou, J., 2021. Porphyry copper and skarn fertility of the northern Qinghai-Tibet Plateau collisional granitoids. Earth-Science Reviews, 214, 103524. https://doi.org/10.1016/j.earscirev.2021.103524

کاربرد آنالیز EPMA در ســـاملنه مس- مولیبدن پورفیری هفت‌چشـــمه به عنوان یک شاخص شیمیایی تعیین منشأ ماگما

شهره حسن پور[1*]، مریم آهنکوب[2]

[1] دانشیار، گروه زمین شناسی، دانشگاه پیام نور، تهران، ایران

[2] استادیار، گروه زمین شناسی، دانشگاه پیام نور، تهران، ایران

[*] مسئول مکاتبات: hassanpour@pnu.ac.ir

تاریخ دریافت: ۱۴۰۱/۱۱/۲۴
تاریخ بازنگری: ۱۴۰۲/۰۶/۰۸
تاریخ پذیرش: ۱۴۰۲/۰۶/۱۹

DOI: 10.22067/econg.2023.81046.1068

سیستم پورفیری مس-مولیبدن پورفیری هفت‌چشمه در زون ماگمایی ارسباران و در زون ساختاری البرز-آذربایجان در شمال غرب ایران قرار گرفته است. از آنجایی که کانه‌زایی در این سیستم پورفیری، عمدتا در استوک‌های گابرودیوریت و گرانودیوریت پورفیری رخ داده است، از ترکیبات شیمیایی کانی‌های تشکیل دهنده این دو استوک پورفیری برای شناسایی فرآیندهای ماگمایی و کانی‌سازی گرمابی در تشکیل آنها استفاده شده است. دماهای اشباع محاسبه شده برای تمام آپاتیت‌ها (ماگمایی و گرمابی) محدوده‌ای از دماهای ۸۳۰ تا ۸۷۷ درجه سانتی‌گراد و فشارهای ۰.۱۱ تا ۰.۹۶ کیلوبار را نشان می‌دهد که مربوط به اعماق ۴ تا ۱۰ کیلومتری و با محتوای H_2O_{melt} (3< wt.%) است و نشان دهنده منشا آنها از یک ماگمای کالک آلکالن آبدار عمیق است. همچنین نتایج آپاتیت‌های تجزیه شده از ماگماهای کانه‌دار نشان می‌دهد که در شرایط اکسیدان بوسیله یک ماگمای نوع I و با fO_2 نسبتاً بالا تشکیل شده‌اند.

بررسی روند تغییرات عناصر فرار نشان داده است که خروج مایع اولیه احتمالاً در دماهای ~ ۷۱۲ تا ۸۴۲ درجه سانتیگراد و تحت تأثیر ماگمای مافیک آبدار و اکسیدان که از قسمت‌های عمیق‌تر یک مخزن ماگمایی منشا گرفته، رخ داده است. تبلور تفریقی آپاتیت‌ها ممکن است در طیف وسیعی از اختلاط ماگمایی گابرودیوریتی و گرانودیوریتی در یک اتاقک ماگمایی رخ داده باشد.

واژه‌های کلیدی: آپاتیت، EPMA، هفت‌چشمه، سیستم پورفیری Cu-Mo، ایران